Journal of the Korean Physical Society, Vol. 76, No. 1, January 2020, pp. 27∼33

A Study on Computational Fluid Dynamic Simulations to Improve the Thickness Uniformity of Porous Metal Films Deposited by Using Cluster Sputtering

Jun Hyeong Kim, Se Yong Park and Hee Chul Lee*
Department of Advanced Materials Engineering, Korea Polytechnic University, Siheung 15073, Korea

Sung Ho Yun
Corporate Research Institute, Kwang Lim Precision Ltd., Daegu 43013, Korea

Ho Nyun Lee
Surface Technology R&D Group, Korea Institute of Industrial Technology, Incheon 21999, Korea

(Received 26 July 2019; accepted 2 October 2019)

We conducted computational fluid dynamic (CFD) simulations to improve the thickness uniformity of cluster-sputtered porous metal films. The cluster sputtering equipment was divided into a module where the sputtered metal atoms condensed and cluster nanoparticles formed and a chamber where porous metal films were deposited. To optimize the equipment geometry, we performed simulations and deposition experiments for various planar nozzle positions and nozzle-to-substrate distances in the module. The simulated gas velocity distribution 25 mm above the substrate exhibited a similar tendency to the thickness distribution of the deposited porous Cu films. When a 4-mm nozzle was located 40 and 240 mm from the module center and substrate, respectively, the simulated gas velocity distribution exhibited uniformity to within 8.4% for the substrate with a 70-mm radius. The thickness uniformity and the deposition rate of the deposited porous Cu films were 9.3% and 2 μm/min, respectively, using equipment with the same geometry.

PACS numbers: 47.11.−j, 78.67.Rb, 78.67.Bf
Keywords: CFD, Porous metal films, Cluster sputtering, Thickness uniformity
DOI: 10.3938/jkps.76.27

I. INTRODUCTION

Porous metal films are metal film materials with a high porosity (*e.g.*, films containing nanosized pores), where their structures are connected to the surface of the material. Recently, porous metal films have attracted attention as next-generation films because of their high surface-to-volume ratios, easy conversion to metal oxides, and their possible applications in the preparation of small, light, and flexible devices [1]. Such porous films can be used in various applications, such as carrying out measurements through molecular recognition due to the selective separation and adsorption reactions of specific substances [2, 3]. In addition, they can be applied in chemical and biosensor areas, such as in biochemical reaction detection [4–6], in energy device areas, such as in high-capacity capacitors, secondary batteries, and fuel cells [7], and in catalysts for accelerating various chemical reactions [8].

Representative existing methods for the formation of porous metal films include de-alloying [9,10], templated deposition [11–14], and solution-based direct deposition [15–17]. The de-alloying method is the most actively studied method, where the formation of alloy films is followed by the removal of one component by using a chemical solution or plasma to give a nanoporous structure. In this instance, the resulting structure is determined by the alloy composition and by phase separation within the alloy. However, this method tends to be limited to chemically or electrochemically stable precious metals, such as gold and platinum, and has a drawback in that the substrate can be damaged by the highly corrosive solution or the high-energy plasma-phase gas species required for component removal. In contrast, the templated deposition method forms porous metal films by using a nanostructured template (*e.g.*, a metal colloid, polystyrene, or silica particles), with the metal film being deposited on top of the template and template being subsequently removed. This method is complicated because the process is divided into several

*E-mail: eechul@kpu.ac.kr

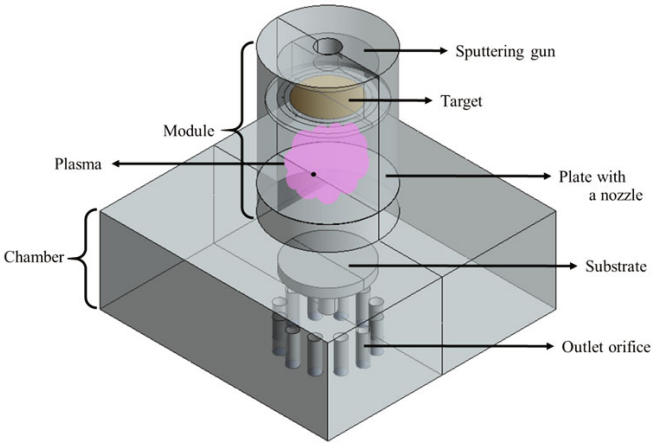

Fig. 1. (Color online) Schematic diagram of the simulation and experimental equipment employed for cluster sputtering.

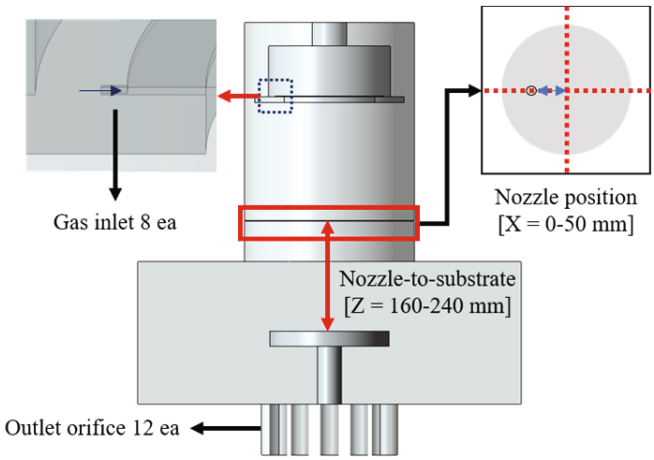

Fig. 2. (Color online) Variations in the equipment dimensions for the simulations and the experiments.

steps and has a drawback in that impurities may form if complete template removal is not achieved. Unlike the above described methods, the solution-based direct deposition method directly forms nanoparticles on a substrate from a solvent-nanoparticle solution. This method can be categorized as electrochemical deposition, sol-gel deposition, or self-assembly, depending on the method of nanoparticle dissolution/formation employed. However, these wet methods are not environmentally friendly due to the generation of waste liquor and have a drawback in that the nanostructure geometry and materials that can be formed are limited.

Thus, we herein wished to examine the use of the environmentally friendly cluster sputtering method for the formation of high-purity porous metal films with less restrictions on deposition materials and less damage to the substrate. Figure 1 shows a schematic representation of the equipment employed for depositing the porous metal films by using cluster sputtering. More specifically, this equipment consists of a cylindrical upper module, in which sputtering and nanocluster particle formation occur, and a rectangular lower chamber, in which the nanoparticles ejected through the nozzle are moved by the gas flow and film deposition occurs. The formed nanocluster particles are combined through sputtering due to the supercooling effect, and these particles are discharged from the module through the nozzle due to a high pressure difference, transported to the substrate, and deposited to form porous metal films. The nozzle is simply a cylindrical hole with a diameter of 4 mm in the plate separating the module and the chamber. As this method is based on sputtering, it can be carried out at room temperature, and the deposition materials and the substrates employed are not limited. In addition, nanostructures can be directly formed without complicated intermediate processes [18]. However, high device development costs are involved because this is a vacuum-based technology, and ensuring uniformity for large area deposition is difficult. Thus, we wish to determine the mechanism by which the formed nanocluster particles are moved by the fluid by means of predictions through computational fluid dynamics (CFD)-based simulations and derivation of related physical values [19]. The velocity distribution of the fluid is then examined while the planar position of the nozzle and the nozzle-to-substrate distance, which are expected to affect the flow of the nanocluster particles significantly, are adjusted. In addition, we attempt to form porous metal films by constructing the same equipment designed earlier, for which a flow analysis is conducted through simulations, and the uniformity of the film thickness is measured according to the deposition position. Finally, the gas velocity distribution in the vicinity of the substrate as calculated through simulations is compared with the thickness uniformity of the deposited films obtained experimentally to find a correlation, and the usefulness of the development of such a cluster sputtering device using flow analysis simulations is discussed.

II. EXPERIMENTS AND DISCUSSION

Figure 2 shows a cross-section of the equipment used in this study, in addition to the ranges of equipment dimensions employed in the simulations and experiments. Eight symmetric gas inlets were distributed for injection to the target surface, and 12 outlet orifices were symmetrically positioned below the substrate in order to form a uniform flow. The pressure of the chamber was fixed at 30 mTorr. As shown in Fig. 2, X, which is the position of the 4-mm-diameter nozzle through which the gas in the module is ejected into the chamber, was varied from the center to positions away from the center by up to 50 mm (X = 0, 30, 40, or 50 mm). In addition, the nozzle-to-substrate distance, Z, was varied from 160 to 240 mm (Z = 160, 180, 210, or 240 mm) in the simulations and the deposition experiments.

Table 1. Simulation and experimental deposition conditions employed herein.

	Computational simulation	Experimental deposition
Module diameter	287 mm	
Chamber size	750 × 750 mm	
Gas inlet	3.79×10^{-6} kg/s	Ar 125 sccm, He 22 sccm
Chamber pressure	30 mTorr	
Nozzle position X	0–50 mm from the center of the plate	
Nozzle-to-substrate distance Z	160–240 mm	
Meshing	1,860,000 hexagonal meshes	-
Sputtering	-	6″ Cu target, DC 400 W

Simulations were conducted using Fluent (v. 19.0, ANSYS Co.), which is software based on the finite volume method that uses the conservation of scalar quantities, such as mass, momentum, and energy, as its governing equations. For the purpose of the simulations, we assumed that the flow was incompressible, that it exhibited a steady-state and standard turbulent motion, and that the plasma did not affect the heat or flow. This assumption was made because the effect of the plasma on the inside of the module was negligible as the pressure difference between the inside of the module and the chamber was large, and the volume expansion and flow that occurred as the nozzle was passed were also particularly large.

The mass flow rate at the inlet was set as the simulation boundary condition and was set to 3.79×10^{-6} kg/s by converting the injected gas flow into a mass. The outlet was fixed to a vacuum of 0 Torr. In the deposition experiment, Ar (125 sccm) and He (22 sccm) were injected. He were used because it promotes the supercooling effect through its high thermal conductivity of 0.151 W/m·K and facilitates the formation of a high-density plasma due to the Penning effect. Moreover, cooling water at a temperature of <10 °C was circulated inside the module wall to accelerate supercooling of the nanoparticles. Table 1 summarizes the conditions employed for the simulations and the experimental deposition procedures.

The planar and the cross-sectional geometries of the deposited porous metal films were captured and examined using field-emission scanning electron microscopy (FESEM, S-430, Hitachi, Japan). The film thicknesses were measured at various points on the SEM image, and average values were calculated. The thickness uniformity on the wafer was defined as follows by using the measured thickness values:

$$\text{Thickness uniformity}(\%) = \frac{t_{max} - t_{min}}{2t_{average}}. \quad (1)$$

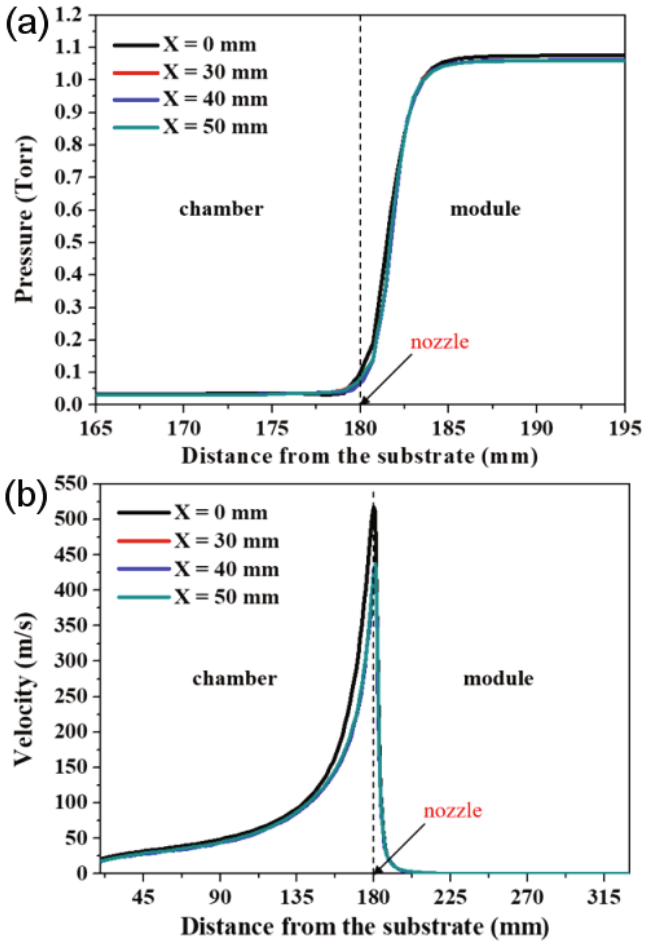

Fig. 3. (Color online) (a) Pressure changes and (b) gas velocity changes of the module and chamber according to the nozzle's position, as obtained through simulations.

Figure 3 shows the changes in the pressure and the gas velocity in the chamber and the module according to the planar position of the nozzle, X, obtained through simulations. As shown in Fig. 3(a), the pressure changes in the module and the chamber were not significant with respect to the nozzle's position. More specifically, when the nozzle was at the center, the pressure difference was slightly higher (*i.e.*, ∼1.05 Torr) than for the other geometries (*i.e.*, ∼1.03 Torr). The pressure inside the module where sputtering occurs is significantly higher than that of the general sputtering process, and the mean free path for the collision of gas particles is as short as several tens of micrometers. Therefore, we concluded that clusters can be easily generated by frequent collisions under conditions where the supercooling of the He atmosphere with a low module wall temperature and a high thermal conductivity is highly likely to occur. In the sputtering equipment fabricated using the same dimensions, the pressure of the module was measured after the same gas had been injected with the pressure of the chamber maintained at 30 mTorr. As a result, an almost identical

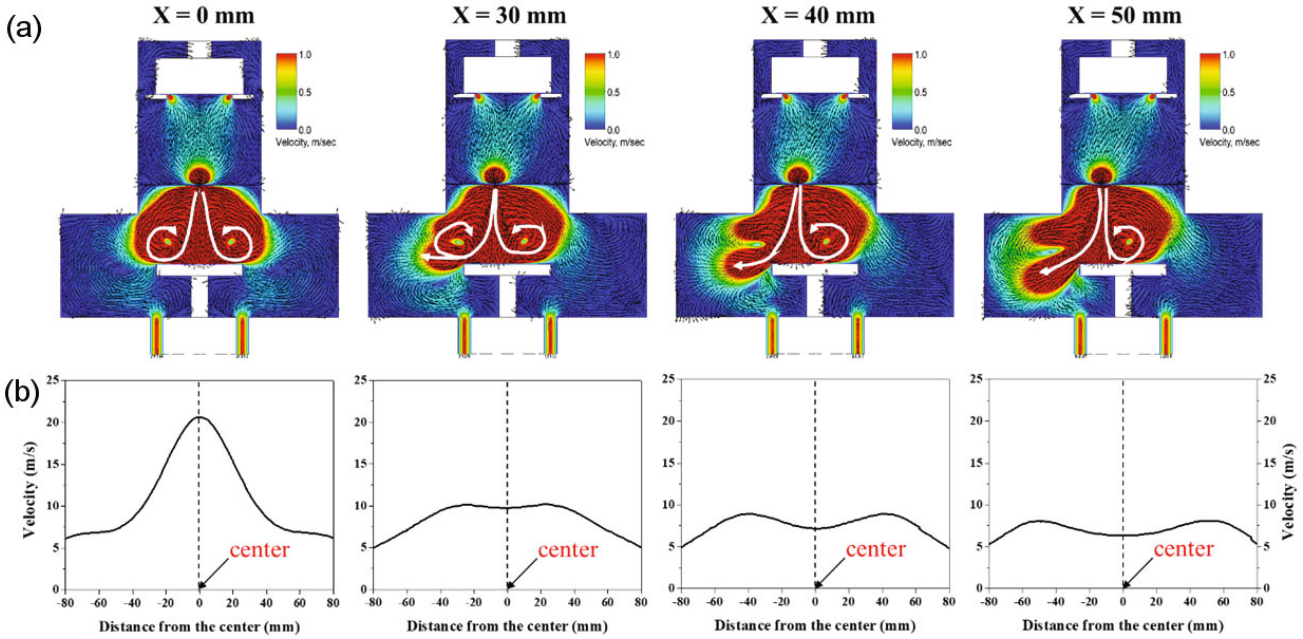

Fig. 4. (Color online) (a) Gas velocity and cross-sectional vector distributions and (b) the gas velocity distribution at a 25-mm height above the substrate through the application of substrate rotation according to the nozzle's position, as obtained through simulations.

pressure was observed. As shown in Fig. 3(b), a particularly high gas velocity was observed at the nozzle due to the large pressure difference between the module and the chamber. More specifically, the velocity was 520 m/s when the nozzle was at the center and 440 m/s when it was at other positions. In addition, the gas velocity was found to decrease significantly when the substrate was closer due to the lack of a pressure difference inside the chamber and to the surface resistance of the substrate and the chamber wall to the gas flow. Owing to this influence of the velocity change, the nanocluster particles are expected to move straight with a high velocity immediately after discharge from the module, although their velocity will significantly decrease as they enter the chamber and move towards the substrate.

Figure 4(a) shows the velocity distribution and the vector directions of gas particles in the cross-sections of the module and the chamber according to the nozzle's position, as determined from CFD simulations. When the nozzle is at the center, two symmetric and clear recirculation centers are formed on the substrate, thereby confirming circulation of the gas. As the nozzle deviates from the center, the gas movement vectors become asymmetric. In addition, for a nozzle position 30 mm from the center ($X = 30$ mm), the left recirculation center could not form a completely closed ellipse, and the vector direction was separated into two. When X was 40 mm, the left recirculation disappeared, and only the right recirculation was formed while for $X = 50$ mm, the left gas velocity vectors significantly deviated from the substrate. Figure 4(b) shows the gas velocity distribution according to the substrate point considering the substrate rotation based on the CFD simulation results of Fig. 4(a). As a no-slip condition was provided to the substrate surface, the velocity distribution at a 25-mm height above the substrate is shown. We assumed that the substrate rotation had no effect on the gas velocity and the vector distribution because the substrate rotated at a slow speed of 5 rpm during this process. To consider the rotation of the deposition substrate, we show the average values of the velocity distributions obtained while the three-dimensional velocity distribution data were rotated at 45° intervals. When the nozzle was at the center ($X = 0$ mm), a large peak was present at the center of the gas velocity distribution curve, and the velocity significantly decreased as the distance from the center increased. When the nozzle was 30 mm away from the center ($X = 30$ mm), a flat area was formed in the middle. When the nozzle was 40 mm or more from the center, two peaks were formed. Thus, as the nozzle position deviated from the center, the average gas velocity gradually decreased, but the uniformity of the gas velocity along the substrate increased.

Figures 5(a) and 5(b) show the gas velocity graph obtained from the simulation and the thickness graph obtained from the deposition experiment, respectively, at various nozzle positions. In the deposition experiment, the condition in which the nozzle was positioned at the center was excluded. A comparison of the two graphs revealed that the changes in the gas velocity and the deposition thickness had similar tendencies. As the nozzle was moved further from the center, both the overall av-

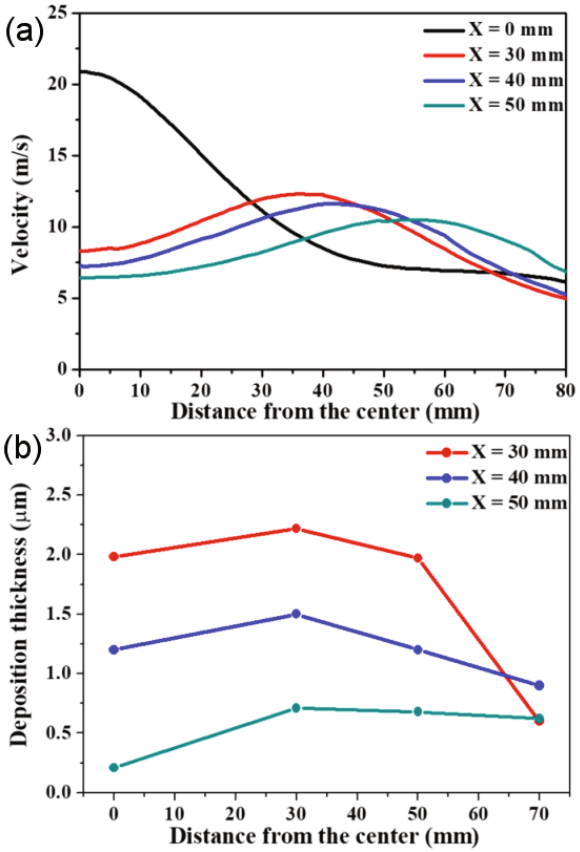

Fig. 5. (Color online) (a) Gas velocity at a 25-mm height above the substrate, as obtained through simulations, and (b) the thickness of the porous copper films, as obtained through the deposition experiment, according to the nozzle's position.

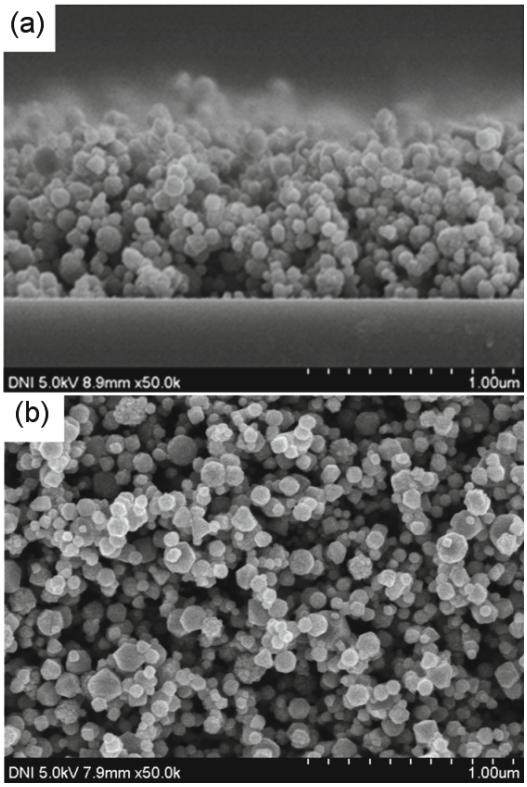

Fig. 6. (a) Surface SEM image and (b) cross-sectional SEM image of the porous copper films obtained from the deposition experiment.

erage gas velocity and the deposition thickness decreased while the uniformity of the gas velocity and the deposition thickness along the substrate increased. This was attributed to the formation of nanoparticle clusters in the module that could be supplied to the substrate at a higher flux at points with a high gas velocity. Moreover, in the porous film growth mechanism taking place during cluster sputtering, the flux at which the nanocluster particles are supplied can determine the deposition thickness of the growing films because the nanoclusters do not have sufficient energy to move on the substrate's surface when they arrive at the substrate.

Figure 6 shows the cross-sectional and the surface SEM images of the porous Cu films deposited using the cluster sputtering equipment fabricated according to the simulation design. Spherical particles in the range of 30-50 nm forming a porous structure were observed, and the films were confirmed not to have been densely formed. The porosity of the porous films calculated through a comparison with the Cu bulk density in consideration of the mass change before and after film deposition, in addition to the average film thickness, was ∼81.8%. Although the thickness varied depending on the nozzle's position and the point of deposition, the surface geometries were comparable. This appears to be because the spherical nanocluster particles had already formed in a shape that could be seen from the films inside the module, and these were then transported and deposited on the substrate by the gas flux.

Figure 7(a) shows the velocity distribution and the vector directions of gas particles in the cross-sections of the module and the chamber according to the nozzle-to-substrate distance, Z. As the previous deposition experiment showed that the thickness uniformity was low when the nozzle's position was $\leq$30 mm from the center and that the deposition rate was particularly low when it was 50 mm from the center, the nozzle was fixed at a position of 40 mm from the center (X = 40 mm), and fluid simulations were performed while the nozzle-to-substrate distance was varied between 160 and 240 mm. As the distance between the target and the substrate was fixed, the space inside the module was reduced when the nozzle-to-substrate distance was increased. The simulation results showed that the pressure difference between the module and the chamber was constant at 1.03 Torr in all cases, and the same pressure difference was measured in the equipment fabricated using the same dimensions. The flow analysis results showed that the number of recirculation centers was two when the nozzle-to-substrate distance was 160 mm (Z = 160 mm), but it decreased to

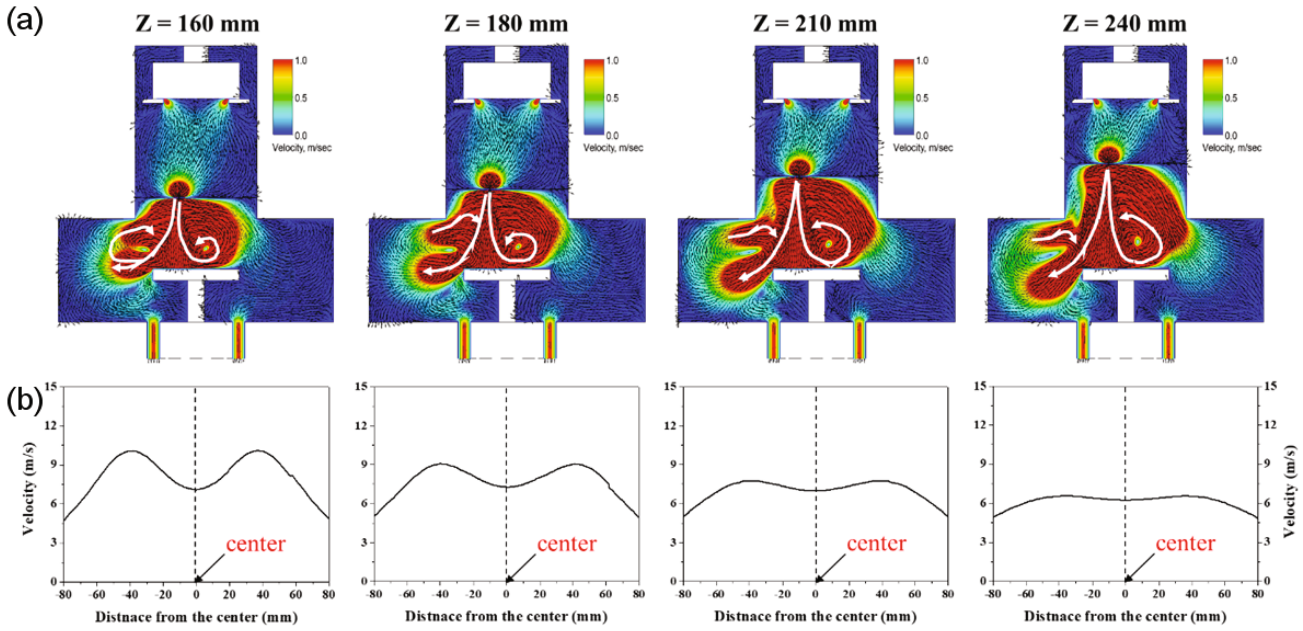

Fig. 7. (Color online) (a) Gas velocity and cross-sectional vector distribution and (b) the gas velocity distribution at a 25-mm height above the substrate through the application of substrate rotation according to the nozzle-to-substrate distance, as obtained through simulations.

one when Z was 180 mm or higher. Moreover, as the distance increased, the recirculation gas flow center moved towards the center of the substrate and the straightness of the velocity vectors that had deviated from the substrate increased. Figure 7(b) shows the gas velocity distribution at a 25-mm height above the substrate considering the substrate rotation based on the CFD simulation results presented in Fig. 7(a). When the nozzle-to-substrate distance was 160 mm, two clear peaks appeared. As the distance were increased, the magnitudes of the peaks decreased, and a flat area appeared in the middle of the substrate. Therefore, the overall average velocity of the gas decreased while the uniformity of the gas velocity increased as the nozzle-to-substrate distance increased. This appears to be because the gas velocity component parallel to the substrate became larger than that perpendicular to the substrate as the nozzle-to-substrate distance was increased, and thereby the center of recirculation moved towards the substrate's center.

Figures 8(a) and 8(b) show the gas velocity graph obtained from the simulation and the thickness graph obtained from the deposition experiment, respectively, with variations based on the substrate point at various nozzle-to-substrate distances. In the deposition experiment, the case with a nozzle-to-substrate distance of 160 mm was excluded. A comparison of the two graphs reveals that the gas velocity change of the simulation and the thickness change of the deposition experiment have similar tendencies, as in the case of the results presented in Fig. 5. As the nozzle-to-substrate distance was increased, both the overall gas velocity and the deposition thickness decreased while the uniformity of both

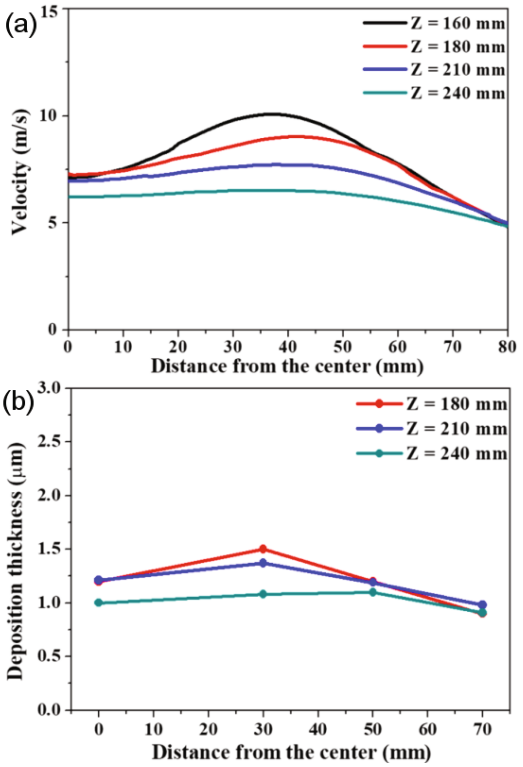

Fig. 8. (Color online) (a) Gas velocity at a 25-mm height above the substrate, as obtained through simulations, and (b) the thickness of the porous copper films, as obtained through the deposition experiment, according to the nozzle-to-substrate distance.

the gas velocity and the deposition thickness along the substrate increased. In particular, when the nozzle-to-substrate distance was 240 mm, the gas velocity change had a high uniformity of 8.4% within the range of 70 mm from the substrate center in the simulation, and the thickness uniformity was within 9.3% in the deposition experiment.

III. CONCLUSION

Computational fluid dynamic (CFD) simulations were conducted to predict the thickness uniformity of porous metal films deposited using cluster sputtering equipment. To verify the usefulness of the simulation, we constructed an actual system by using the optimized simulated conditions, and we deposited porous copper films. The planar position of the nozzle in the module and the nozzle-to-substrate distance were found to affect significantly the gas velocity and the vector distribution in the simulation, as well as the deposition rate and the thickness uniformity of the porous copper films in the actual cluster sputtering system. In particular, we confirmed that the gas velocity distribution at a 25-mm height above the substrate in the simulation and the thickness distribution of the porous Cu films in the actual deposition system exhibited similar tendencies. The porous Cu films deposited by using the experimental deposition system with the same optimal conditions obtained through simulations exhibited a uniformity of 4.7% within a radius of 50 mm from the substrate's center and a uniformity of 9.3% within 70 mm; the average deposition rate was 2 μm/min. The CFD simulation performed in this study is expected to be of particular use in the development of experimental equipment as it was demonstrated to predict successfully changes in the deposition rate and the thickness uniformity of porous metal films deposited by using cluster sputtering.

ACKNOWLEDGMENTS

This work was supported by the Industrial Technology Innovation Program (No. 10077465) funded by the Ministry of Trade, Industry, and Energy (MOTIE) and by the Priority Research Center Program (NRF-2017 R1A6A1A03015562) funded by the Ministry of Education (MOE) of the Republic of Korea.

REFERENCES

[1] F. Jia, C. Yu, K. Deng and L. Zhang, J. Phys. Chem. C **111**, 8424 (2007).
[2] Y. Jiao *et al.*, Nanotechnology **22**, 295 (2011).
[3] X. Y. Lang *et al.*, Appl. Phys. Lett. **94**, 213109 (2009).
[4] H. T. Tran, J. Y. Byun and S. H. Kim, J. Alloys Compd. **764**, 371 (2018).
[5] L. Zhang *et al.*, ACS Nano **7**, 4595 (2013).
[6] S. Park, T. D. Chung and H. C. Kim, Anal. Chem. **75**, 3046 (2003).
[7] X. Y. Lang, H. T. Yuan, Y. Iwasa and M. W. Chen, Scr. Mater. **64**, 923 (2011).
[8] H. Y. Jung *et al.*, Adv. Energy Mater. **1**, 1126 (2011).
[9] Z. Zhang *et al.*, J. Phys. Chem. C **113**, 12629 (2009).
[10] G. H. Lee *et al.*, Thin Solid Films **631**, 147 (2017).
[11] P. Jiang, J. Cizeron, J. F. Bertone and V. L. Colvin, J. Am. Chem. Soc. **121**, 7957 (1999).
[12] E. Metwalli *et al.*, Langmuir **25**, 11815 (2009).
[13] J. Patel *et al.*, Anal. Chem. **85**, 11610 (2013).
[14] B. Zhao and M. M. Collinson, J. Electroanal. Chem. **684**, 53 (2012).
[15] Y. Lu, Q. Wang, J. Sun and J. Shen, Langmuir **21**, 5179 (2005).
[16] D. Van Noort and C. F. Mandenius, Biosens. Bioelectron. **15**, 203 (2000).
[17] J. Jia, L. Cao and Z. Wang, Langmuir **24**, 5932 (2008).
[18] A. F. Jankowski and J. P. Hayes, J. Vac. Sci. Technol. A **21**, 422 (2003).
[19] U. H. Kwon, S. H. Choi, Y. H. Park and W. J. Lee, Thin Solid Films **475**, 17 (2005).